

Geomechanical Properties of Shear Zones in the Eastern Aar Massif, Switzerland and their Implication on Tunnelling

By

S. Laws^{1,2}, E. Eberhardt², S. Loew², and F. Descoeurdes³

¹Dr. Heinrich Jäckli AG, Zürich, Switzerland

²Engineering Geology, Swiss Federal Institute of Technology (ETHZ), Zürich, Switzerland

³Department of Civil Engineering, Swiss Federal Institute of Technology (EPFL),
Lausanne, Switzerland

Received December 17, 2001; accepted January 9, 2003

Published online April 29, 2003 © Springer-Verlag 2003

Summary

Rock zones containing a high fracture density and/or soft, low cohesion materials can be highly problematic when encountered during tunnel excavation. For example in the eastern Aar massif of central Switzerland, experiences during the construction of the Gotthard highway tunnel showed that heavily fractured areas within shear zones were responsible for overbreaks in the form of chimneys several metres in height. To understand and estimate the impact of the shear zones on rock mass behaviour, knowledge concerning the rock mass strength and deformation characteristics is fundamental. A series of laboratory triaxial tests, performed on samples from granite- and gneiss-hosted shear zones revealed that with increasing degree of tectonic overprint, sample strength decreases and rock behaviour shows a transition from brittle to ductile deformation. These trends may be explained by increasing fracture densities, increasing foliation intensity, increasing thickness of fine-grained, low cohesion fracture infill, and increasing mica content associated with the increasing degree of tectonic overprint. As fracture density increases and the influence of discrete, persistent discontinuities on rock mass strength decreases, behaviour of the test samples becomes more and more representative of rock mass behaviour, i.e. that of a densely fractured continuum. For the purpose of numerical modeling calculations, the shear zones may be subdivided with respect to an increasing fracture density, foliation intensity and mica content into a strongly foliated zone, a fractured zone and a cohesionless zone, which in turn exhibit brittle, brittle-ductile and ductile rock mass constitutive behaviour, respectively.

Keywords: Shear zones, strength and deformation characteristics, laboratory triaxial tests, rock mass properties, tunnelling conditions.

1. Introduction

Rock zones containing a high fracture density and/or soft, low cohesion materials can be highly problematic when encountered during tunnel excavation. Experience in such

zones has shown that the highly fractured and almost cohesionless nature of the rock mass may result in tunnel face instability, excessive overbreak and/or large deformations due to squeezing (e.g. Deere, 1973; Müller, 1978; Keller and Schneider, 1982; Schubert, 1993; Schubert and Riedmüller, 1997, 2000). Extreme water inflows frequently aggravate such instabilities.

In the eastern Aar massif of central Switzerland, construction is currently underway for the new 57 km Gotthard Base Tunnel (Fig. 1). Loew et al. (2000) describe the geologically controlled hazards expected during tunnel construction, chief amongst which relate to shear zones. Experiences during the construction of the nearby Gotthard highway tunnel (Fig. 1) showed that heavily fractured areas within shear zones were responsible for overbreaks in the form of chimneys several metres in height (Keller et al., 1987).

To enable the rigorous planning and design of deep alpine tunnelling projects, including the selection of construction methods and the determination of suitable support requirements and safety regulations, it is essential to estimate the impact of the shear zones on rock mass stability. Knowledge concerning shear zone/rock mass strength and deformation characteristics is also required to properly incorporate the effects of the shear zone within analytical and numerical design methodologies.

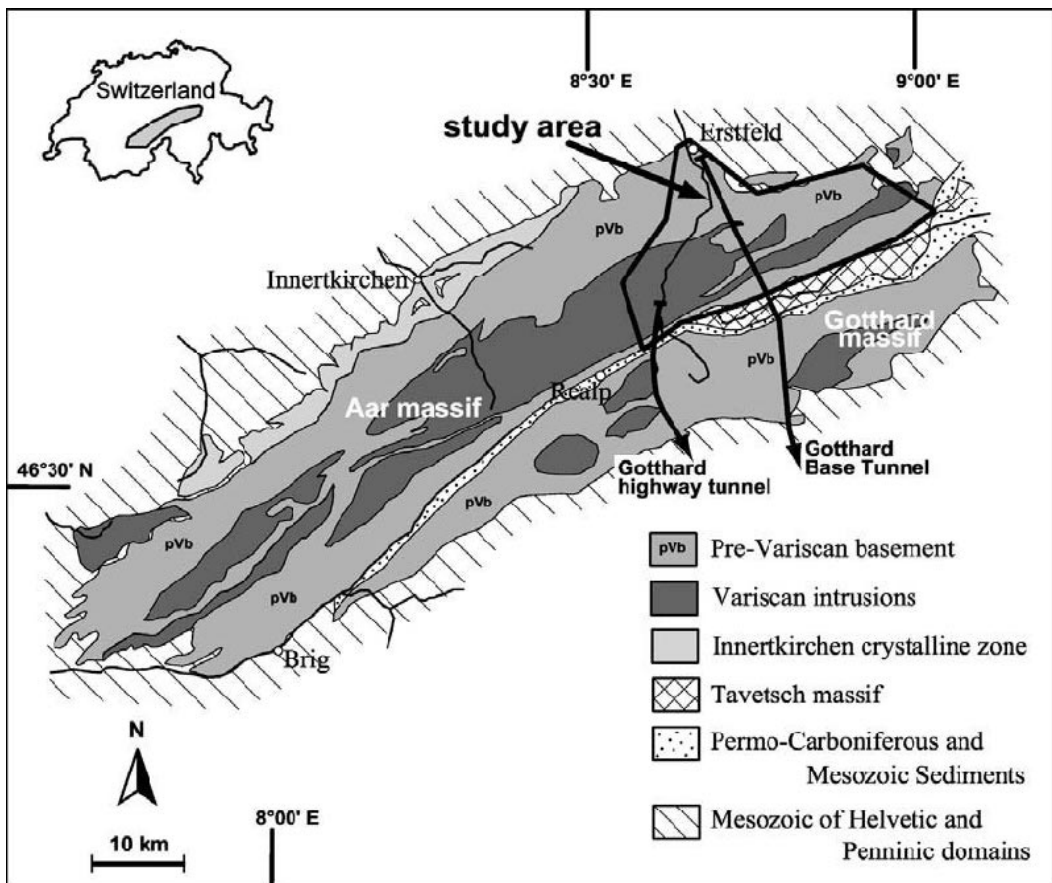


Fig. 1. Geographical and geological setting of the Aar Massif (after Abrecht, 1994), showing location of the study area, Gotthard Base-Tunnel and Gotthard Highway Tunnel

Previous studies examining the geomechanical properties of heavily fractured rock masses, especially fault zones, have shown that rock strength and deformation parameters vary depending on the different structural characteristics (e.g. fracture density) within the zone (e.g. Chester and Logan, 1986; Habimana et al., 2002). In general, it is assumed that with increasing fragmentation there is a reduction in rock strength and Young's modulus, and an increase in plastic deformation.

Shear zones in the eastern Aar massif have been widely studied, but mostly with respect to their spatial distribution (e.g. Jäckli, 1951; Eckardt, 1957; Steck, 1968b; Eckardt et al., 1983; Keller et al., 1987; Schneider, 1993). Given the high degree of correlation between these features and ground control problems encountered during the construction of the Gotthard highway tunnel, it is surprising that the geomechanical properties and their variance within the shear zones have not been rigorously studied. In fact, studies examining the geomechanical properties of such heavily fractured shear zones and fault zones and relating these properties to the structural characteristics are generally rare.

This paper presents the results of an extensive investigation into the geomechanical properties of shear zones in the eastern Aar massif and their dependence on structural characteristics. However, the methodologies and results obtained are also highly relevant to fractured zones in general, when hosted in crystalline rock masses. The paper first describes the structure of the shear zones and then presents results from a series of triaxial compression tests performed on samples with varying degrees of tectonic damage. The analysis concentrates on the description of the rock behaviour with respect to the applied stress and includes the determination of elastic constants and Mohr-Coulomb strength parameters. Variations in rock behaviour and the validity of the parameter values obtained are assessed with respect to the structural composition of the shear zones.

2. Shear Zone Structure and Characteristics

2.1 General Characterization of Shear Zones

Shear zones are narrow zones of highly strained rock characterized by spatial gradients of finite strain. The amount of strain is generally highest within the centre of the shear zone, decreasing outward into the wall rocks adjacent to the zone. Another characteristic feature is their anastomosing geometry, encompassing and wrapping around more rigid, less deformed rock bodies (i.e. shear lenses).

Four general types of shear zones can be defined, based on the dominating type of deformation (e.g. Ramsay and Huber, 1987; Davis and Reynolds, 1996):

- *Ductile* shear zones display structures that have a metamorphic aspect and record shearing by ductile flow. The deformation processes within ductile shear zones are mainly achieved by crystal plasticity and thus involve only a minor amount of fracturing. These rocks are often referred to as mylonites (e.g. Passchier and Trouw, 1996).
- *Brittle* shear zones, generally termed fault zones, contain fractures and other features formed by brittle deformation mechanisms. Displacement occurs along a

network of closely spaced fractures. Due to the high permeability of the fractured material, hydrothermal inflow is promoted and faulting is often accompanied by hydrothermal activity (e.g. Hulin, 1929; Higgins, 1971; Sibson, 1977; Wise et al., 1984).

- *Semibrittle* shear zones include *en échelon* veins or joints and stylolites and involve mechanisms such as cataclastic flow and pressure solution.
- *Brittle-ductile* shear zones show evidence for both brittle and ductile deformation.

2.2 Characterization of Shear Zones in the Eastern Aar Massif

2.2.1 Geological Setting

The Aar massif is situated in the central Swiss Alps and outcrops in the form of a 115 km long and 23 km wide NE striking mountain range. The study area is located in the eastern part of the massif (Fig. 1). The Aar massif is built up by magmatic rocks (dominantly granites) enclosed in an older crystalline basement (primarily gneisses). Rocks and structures in the Aar massif are characterized by an overprint of the Tertiary Alpine collision during which the rocks were affected by heterogeneous ductile deformation and metamorphism under, at most, medium greenschist facies/biotite zone conditions (Labhart, 1977; Steck, 1984; Choukroune and Gapais, 1983; Frey et al., 1980). The deformation was localized on all scales, from millimetre to kilometre, in ductile and brittle-ductile shear zones (Choukroune and Gapais, 1983; Meyer et al., 1989). During subsequent deformation stages (uplift) the Aar massif was affected by brittle processes, which generated shear fractures and joint systems locally filled with hydrothermal crystallizations (Steck, 1968a; Meyer et al., 1989; Bossart and Mazurek, 1990). Due to the preferential weakness of existing shear zones, most brittle fractures concentrated within mylonites. Today, uplift of the Aar massif is still ongoing (Pavoni, 1979; Gubler et al., 1981; Kahle et al., 1997) and quaternary movements are assumed to be bound to isolated shear zones (Jäckli, 1951; Eckardt, 1957; Eckardt et al., 1983; Fischer, 1990).

2.2.2 Structural Composition

The majority of shear zones in the eastern Aar massif are between 2 and 15 m wide, strike ENE–WSW and dip steeply to the S or N (Laws et al., 2003). A minor shear zone set strikes NW–SE and dips steeply to the SW or NE.

The deformation structures associated with these shear zones were found by Laws et al. (2003) to be primarily ductile. A characteristic progressive evolution from the host rock to mylonite (rocks with 50 to 90% matrix relative to the porphyroclast content) and locally ultramylonite (rocks with more than 90% matrix) is documented by the formation and intensification of a foliation and a stretching lineation and the progressive replacement of the host rock by a finer-grained material containing newly crystallized and recrystallized minerals. Rock compositions simultaneously show an increase in the mica content. Towards the mylonitic and ultramylonitic zones, the network of small-scale shear zones anastomosing around more competent, lozenge-shaped lenses increases in frequency.

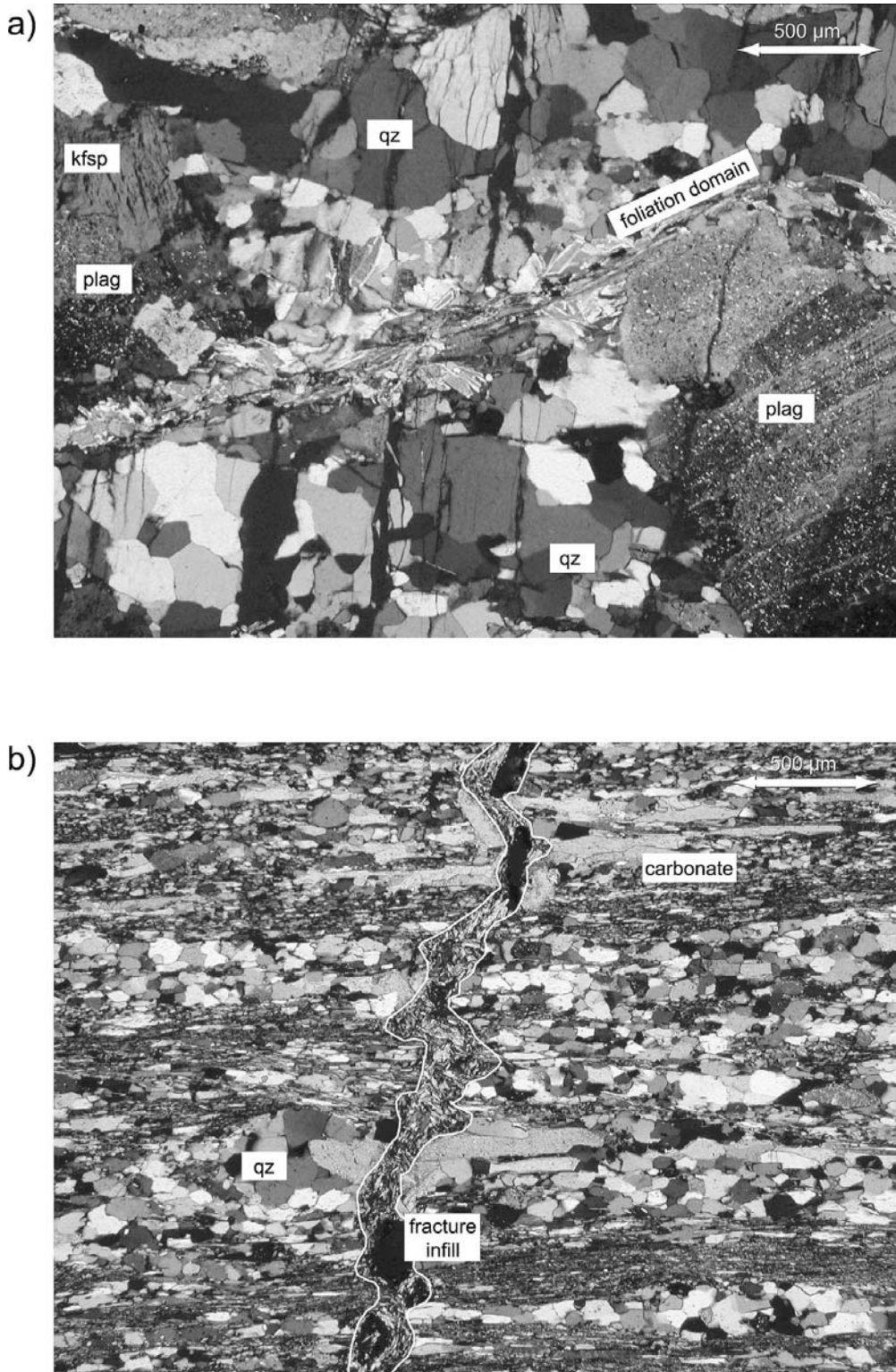


Fig. 2. a) Transgranular open fractures intersecting quartz (*qz*) and feldspar (*plag*, *kfsp*) minerals and finer-grained foliation domains. Thin-section is taken from a granite-hosted shear zone sample (GR3, borehole Ia); b) Transgranular fracture showing an infill of fine-grained quartz, biotite, muscovite and carbonate arranged in a structureless manner. Thin-section is taken from the corresponding gneiss-hosted shear zone sample (GN3, borehole IIa). Thin sections show a cut perpendicular to foliation and parallel to stretching lineation (crossed polars)

The shear zones additionally show a higher fracture density than the host rock (Laws et al., 2003). The fractures oriented parallel and oblique to the foliation can be open but are mainly filled with a μm -thick, almost cohesionless, fine-grained, structureless arrangement of micas and quartz. Microfractures represent trans- and intra-granular fractures (Fig. 2). The highest fracture densities are restricted to fine-grained and strongly foliated sections of the shear zone. In addition to fracture density, the thickness of the fracture infill generally increases towards areas with highest fracture densities, rendering the mylonite more and more friable. In heavily fractured zones, foliation is destroyed by the fracturing and structureless, low cohesion microbreccias occur. The microbreccias consist of mylonite fragments separated by a mm-wide, fine-grained matrix. The matrix is composed of the same material as the fracture infilling and is therefore assumed to be representative of the infill.

2.2.3 Structural Model

Laws et al. (2003) examined more than 100 shear zones in the eastern Aar massif and found that in most cases, three different textural subzones can be characterized within the shear zones based on fracture density and mica content. With increasing fracture density and mica content, these include a *strongly foliated zone*, a *fractured zone* and a *heavily fractured, cohesionless zone* (Fig. 3). The strongly foliated zone forms approximately 50% of the total shear zone width, with the fractured and cohesionless zones forming 40% and 10%, respectively. The thickness of these intervals may vary along strike and dip depending on the degree of ductile and/or brittle control on the formation of the shear zone. The zones are oriented approximately parallel to the rock mass foliation and often form a symmetric sequence centred by the heavily fractured, cohesionless zone. The cohesionless zone may also anastomose within the fractured zone, or may be absent all together.

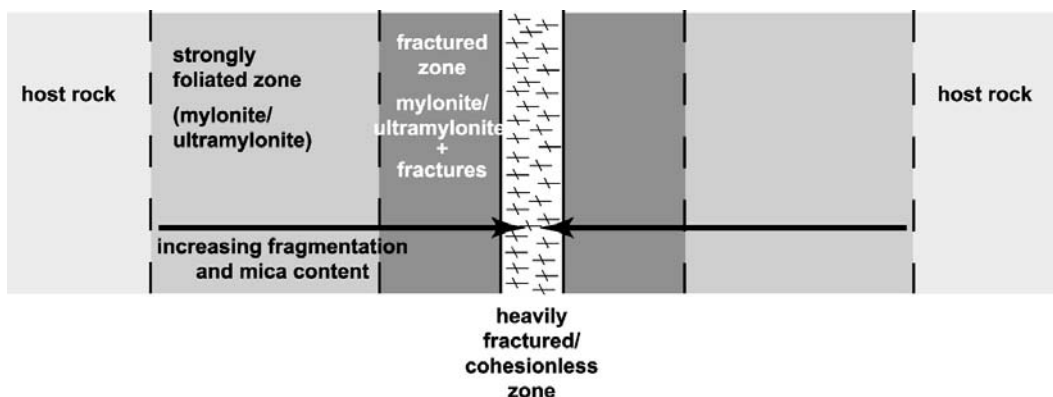
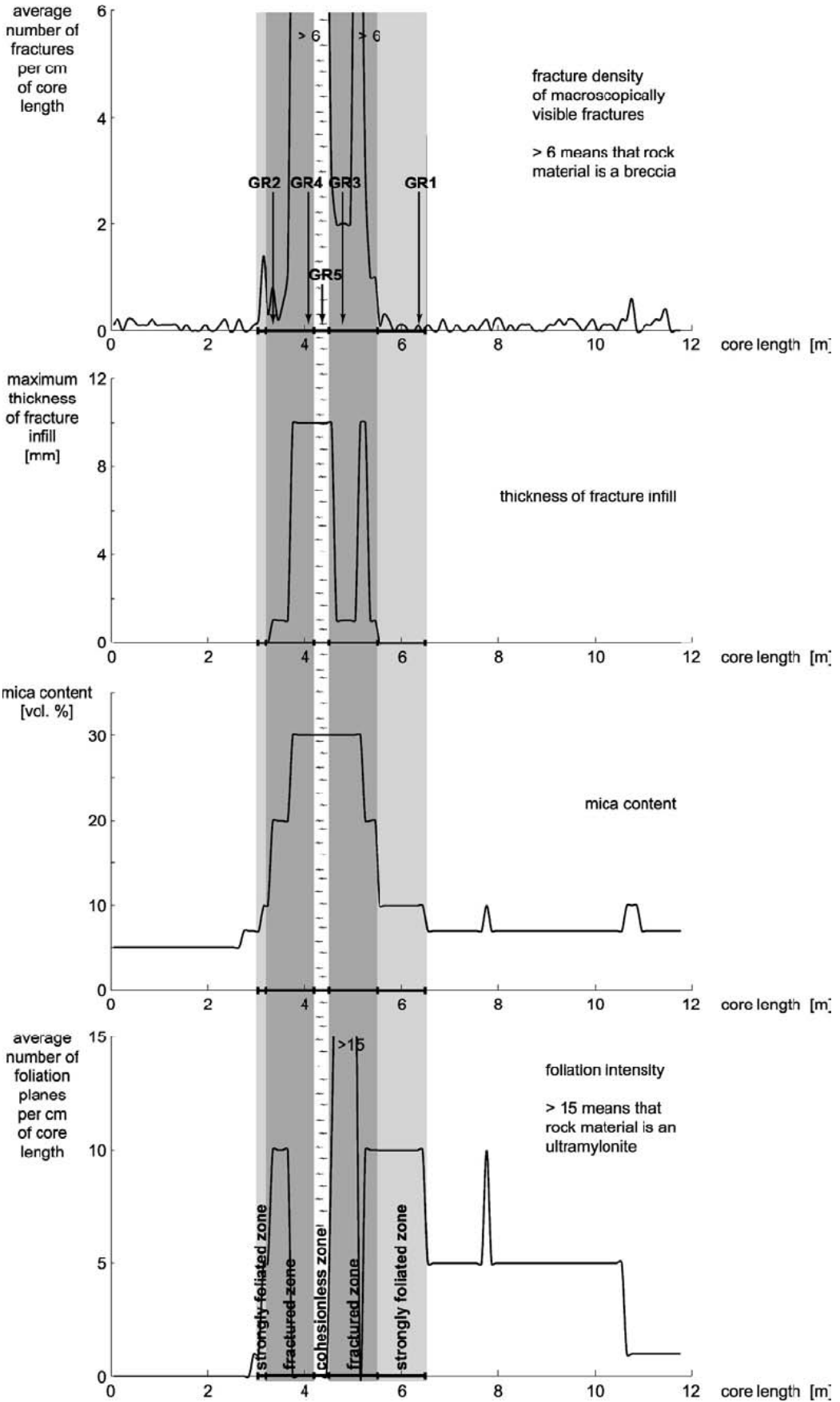


Fig. 3. Schematic illustration of the structural composition of shear zones in the eastern Aar massif

Fig. 4. Fracture density, thickness of fracture infill, mica content and foliation intensity measurements along a transect crossing a granite-hosted shear zone (borehole Ia). Figure also shows the sampling locations for samples GR1–GR5



The *strongly foliated zone* has thicknesses of up to several metres and is characterized by mylonites/ultramylonites slightly more fractured than the host rock. The strongly foliated zone gradually progresses into the *fractured zone*, which in turn may be a few metres thick. Like the strongly foliated zone, the fractured zone is composed of mylonite or ultramylonite, but is more intensely fractured. Some fractures contain infills with thicknesses of up to 1 mm, with increasing thicknesses correlating to an increase in the amount of mica in the rock material. Due to the high degree of fragmentation in the fractured zone and the thickness of the fracture infill, the rock material can be extremely friable. Extremely strong fragmentation towards the heavily fractured, cohesionless zone may result in the disruption of the rock fabric. Under these circumstances a structureless microbreccia is formed consisting of cubic centimetre sized fragments of mylonite separated by a millimetre thick fine-grained matrix. Microbreccias found within the fractured zone may have a relatively strong cohesion, which would have formed secondarily.

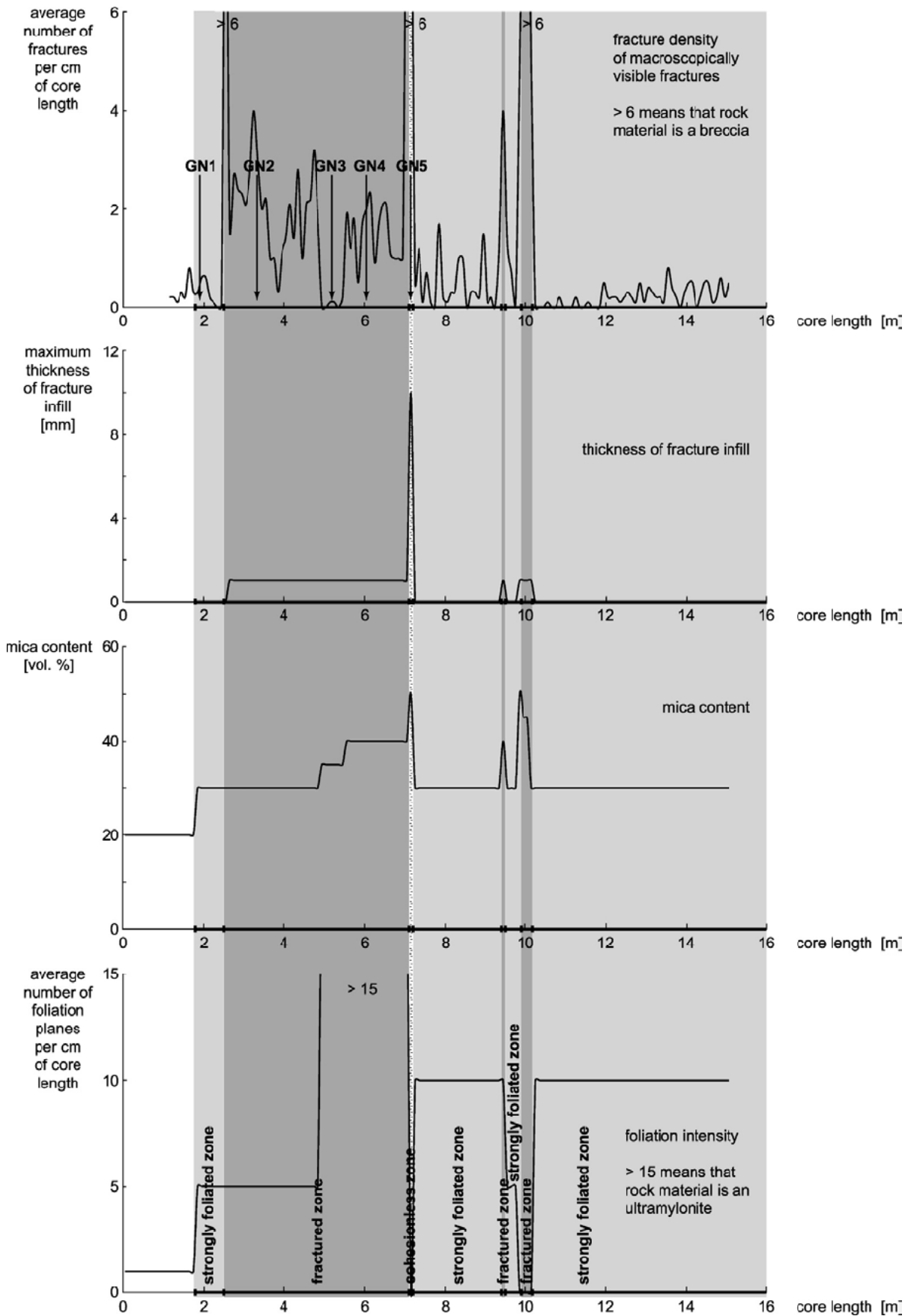
The *cohesionless zone* has a distinct and sharp contact with the surrounding cohesive material. The thickness of the zone varies from a few centimetres to several decimetres. The cohesionless zone consists of structureless microbreccias that can be distinguished from those of the fractured zone by the increased amount of matrix material and by their almost cohesionless nature. The rock material in this zone shows some signs of cohesion due to the fine-grained and interlocking nature of rock fragments and matrix minerals. Swelling clay minerals were not observed.

2.2.4 Examples

Figures 4 and 5 show examples of the distribution of fracture density, thickness of fracture infill, mica content and foliation intensity across granite- and gneiss-hosted shear zones in the eastern Aar massif. It should be noted that the distribution of fracture density in these diagrams is based only on macroscopically visible fractures. Microfractures also play an important role in the rock's behaviour, and in the case of the fine-grained shear zone materials (e.g. ultramylonites), a significantly high density of microfractures exists.

Inspection of the trends for the granite-hosted shear zones (Fig. 4) shows that the density of visible fractures is high in the fractured zone and increases towards the heavily fractured, cohesionless zone. This is also true for the microfractures. In contrast, the fracture density in the gneiss-hosted shear zone (Fig. 5) is less regular, but does show a high number of macroscopically visible fractures at the different transition boundaries between the strongly foliated and fractured zones. This number decreases within the strongly foliated zone intervals, but increases again within the heavily fractured, cohesionless zone. With respect to the microfracture density in the gneiss-hosted shear zones, numbers based on thin-section analyses are low at the transition from the strongly foliated to the fractured zone but then constantly increase towards the heavily fractured, cohesionless zone.

Fig. 5. Fracture density, thickness of fracture infill, mica content and foliation intensity measurements along a transect crossing a gneiss-hosted shear zone (borehole IIa). Figure also shows the sampling locations for samples GN1–GN5



3. Triaxial Testing

To determine the geomechanical properties of the materials representing these different shear zone intervals, as described in the previous section, a series of laboratory triaxial tests were performed on samples taken from the eastern Aar massif. The tests were performed at the rock mechanics laboratory (LMR) of the Swiss Federal Institute of Technology, Lausanne (EPFL).

3.1 Sampling and Sample Preparation

Samples were obtained from two boreholes drilled across two shear zones intersecting the safety tunnel of the Gotthard highway tunnel (Figs. 6, 7). The first borehole was drilled through a shear zone within the Aar granite (borehole Ia), and the second was drilled through a shear zone in gneiss (borehole IIa). Both shear zones had been sites of overbreaks during tunnel construction, with overburdens of 400 and 500 m respectively.

The boreholes were oriented normal to the strike and dip of the shear zones and rock mass foliation. To minimize sample disturbance and the effects of sample heterogeneity on the planned laboratory tests, relatively large diameter cores were drilled to obtain 90 mm diameter test samples. To protect the weaker rock intervals, triple-tube drilling flushed with a minimal amount of water was performed. Samples were then sealed and stored in plastic tubing.

Descriptions of the samples tested are given in Table 1 and are illustrated in Figs. 11 and 12. For testing purposes, one sample was taken from each shear zone subzone for both the granite- and gneiss-hosted shear zones, with the exception of the fractured zone, where several samples were taken given the increasing fracture density towards the cohesionless zone. Sampling locations with respect to the shear zone structure are shown in Figs. 4 and 5. All samples were oriented with their core axis normal to the foliation.

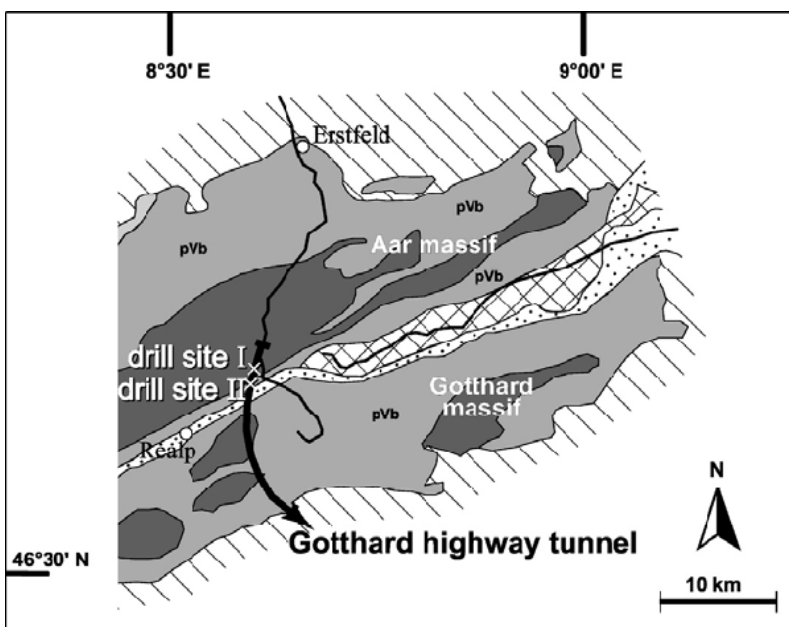


Fig. 6. Drill site locations for boreholes Ia and IIa (see Fig. 1)



Fig. 7. Sub-horizontal triple-tube drilling normal to the strike and dip of the shear zone

Due to the highly fragmented nature of some samples, sample disturbance had to be controlled by leaving the samples in their PVC liner during end preparation. Sample ends were cut through the plastic tubing to form flat, right-angled ends. Samples were removed from the plastic tubing only after end preparation and were supported, where necessary, with adhesive tape and a calcite-based paste (HILTI MD 2000). For samples GN5a-c, it was necessary to drill smaller diameters (55 to 85 mm) than the 90 mm diameter used otherwise. For all samples, ISRM standards (ISRM, 1983) were met with respect to having sample diameters 10 times greater than the maximum grain size or fissure spacing, and with having sample height to diameter ratios greater than two.

3.2 Test Setting, Load Path and Parameters Calculated

Triaxial consolidated, drained compression tests (CD tests) were performed to minimize the effects of excess pore pressures, as samples were tested with their natural water contents to prevent any disturbance to the rock structure associated with drying. Tests were performed according to ISRM guidelines (ISRM, 1983). The loading system consisted of a servo-controlled, stiff testing machine with a maximum load capacity of 200 tonnes. Both LEGEP and HOEK type triaxial cells were used.

Axial loads were applied at a constant displacement rate of 0.1 mm/min, except for samples GN5a-c which were loaded at a rate of 0.2 mm/min. Initial confining pressures were set at 5 MPa, with the exception of specimen GN3b where a confining pressure of 1 MPa was used. Loading was applied until the peak strength was reached, after which a form of controlled multiple failure state loading was employed. This procedure involves periodically increasing the confining pressure to maintain different limit equilibrium states (Kovári and Tisa, 1975). In contrast to Kovári and Tisa's (1975) work, where such loading paths were interpreted as being those for peak strength conditions, results from these tests were interpreted as representing residual strength conditions instead. The reasoning for this was that at peak strength a permanent change

Table 1. Description of granite-hosted (GR) and gneiss-hosted (GN) shear zone samples

	Shear zone unit	Predominant minerals	Rock material properties	Density of macroscopically visible fractures
GR1	strongly foliated zone	~60 vol.% qz, ~30 vol.% fsp, ~10 vol.% mica	mylonite; cm- to mm-spaced foliation, fine-grained (most grains in foliation domains have diameters <0.2 mm)	no visible fractures
GR2	fractured zone	~60 vol.% qz, ~20 vol.% fsp, ~20 vol.% mica	mylonite; mm-spaced foliation, fine-grained (most grains in foliation domains have diameters <0.15 mm)	cm-spaced fractures oriented mainly parallel to foliation, fractures can have an up to 1 mm thick infill
GR3	fractured zone	~60 vol.% qz, ~20 vol.% fsp, ~20 vol.% mica	ultramylonite; mm-spaced foliation, extremely fine-grained (most grains in foliation domains have diameters <0.1 mm)	cm-spaced fractures oriented mainly parallel to foliation, high density of microfractures, fractures can have an up to 1 mm thick infill
GR4	fractured zone	~60 vol.% qz, ~15 vol.% fsp, ~25 vol.% mica	heavily fragmented material; cohesive microbreccia	about 1 cm-large rock fragments in fine-grained, cohesive matrix, high density of microfractures
GR5	heavily fractured, cohesionless zone	~60 vol.% qz, ~15 vol.% fsp, ~25 vol.% mica	heavily fragmented material; cohesionless microbreccia	about 1 cm-large rock fragments in fine-grained, mm-thick, cohesionless matrix
GN1	strongly foliated zone	~60 vol.% qz, ~20 vol.% fsp, ~20 vol.% mica	mylonite; cm- to mm-spaced foliation, fine-grained (most grains in foliation domains have diameters <0.05 mm)	1–2 discrete fractures oriented parallel and oblique to foliation
GN2	fractured zone	~60 vol.% qz, ~10 vol.% fsp, ~30 vol.% mica	mylonite; cm- to mm-spaced foliation, fine-grained (most grains in foliation domains have diameters <0.05 mm)	cm- to mm-spaced fractures oriented parallel and oblique to foliation, fractures can have μ m-thick infills
GN3a, b	fractured zone	~60 vol.% qz, ~5 vol.% fsp, ~35 vol.% mica	ultramylonite; mm-spaced foliation, extremely fine-grained (most grains in foliation domains have diameters <0.01 mm)	cm-spaced fractures oriented mainly parallel to foliation, fractures can have μ m-thick infills
GN4	fractured zone	~60 vol.% qz, ~40 vol.% mica	ultramylonite; mm-spaced foliation, extremely fine-grained (most grains in foliation domains have diameters <0.01 mm)	cm- to mm-spaced fractures oriented parallel and oblique to foliation, high density of microfractures, fractures can have mm-thick infills
GN5a, b, c	heavily fractured, cohesionless zone	~55 vol.% qz, ~45 vol.% mica	heavily fragmented material; cohesionless microbreccia	cm- to mm-large rock fragments in fine-grained, mm-thick, cohesionless matrix

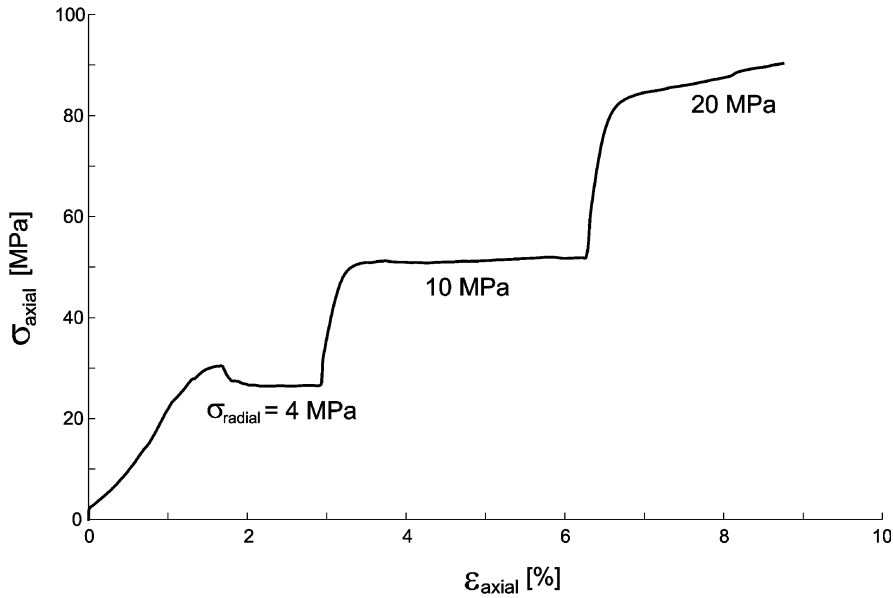


Fig. 8. Example of multi-stage loading path applied during triaxial testing (sample GR4)

to the rock’s fabric occurs through the formation of a shear plane. Therefore, any subsequent loading conditions can only be applicable to that of a residual shear strength state. Confining pressures were increased and held constant two times in succession from 5 to 10 MPa, and again from 10 to 15/20 MPa until residual strengths at these loading intervals were reached (Fig. 8).

Axial strain (ϵ_{axial}) was measured using a linear displacement transducer and volumetric strain (ϵ_v) was established through volume changes to the confining pressure fluid in the triaxial cell. From these parameters, the radial strain (ϵ_{radial}) was determined assuming axial symmetry of a cylindrical volume:

$$\epsilon_v = \epsilon_{axial} + 2\epsilon_{radial} \quad \text{or} \quad \epsilon_{radial} = 0.5(\epsilon_v - \epsilon_{axial}). \quad (1)$$

The validity of this assumption was found to be somewhat limiting given the inhomogeneous nature of the deformations observed in most of the tested specimens.

Approximations of the Young’s modulus (E) were calculated from the axial stress-strain curves as: (1) a Tangent modulus (E_T), i.e. the slope of the axial stress-strain curve at 50% of the peak strength, and (2) a Secant modulus (E_S), taken as the slope of a straight line joining the origin of the axial stress-strain curve to the point at 50% of the peak strength. Values of Poisson’s ratio (ν) were determined by dividing E_T through the slope of the $\sigma_1 - \epsilon_{radial}$ curve at 50% of peak strength. Calculations of the elastic constants were restricted to assumptions of isotropy due to limitations in sampled core orientations. Preferably, a transverse isotropic model would have been more appropriate given the strongly foliated nature of the shear zone rocks.

Through the testing procedure and load paths applied, a linear Coulomb residual strength envelope could be obtained for each sample tested. This envelope was calculated using a linear regression fitting routine (Shah and Hoek, 1991) to establish the residual cohesion (c_r) and residual internal friction angle (ϕ_r). In practice, the assumptions inherent in the use of a linear Coulomb strength envelope (e.g. the development of a discrete, continuous shear plane) can be an oversimplification when applied to the

peak strength conditions for most rock types. However, Brady and Brown (1993) suggest that the criterion does provide a relatively good representation of the residual strength conditions, as strength values tend to increase with increasing shear plane roughness or with the development of multiple shear planes. This is of practical importance and highly relevant to the samples tested given the varying degrees of fracturing represented by the different shear zone rock types.

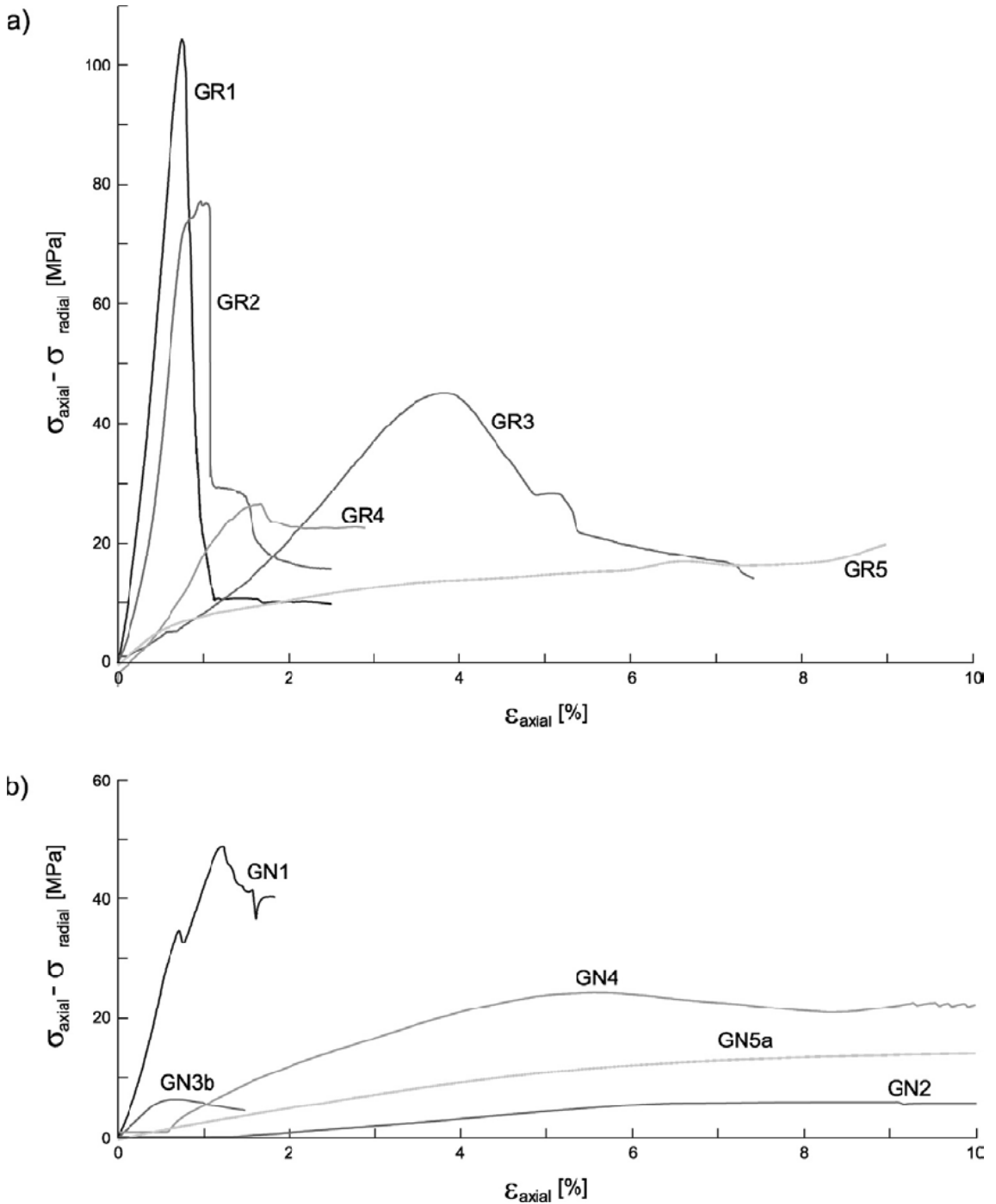


Fig. 9. Stress-strain curves for test samples from: **a)** granite-hosted shear zone; **b)** gneiss-hosted shear zone

Table 2. Summary of test results; where E_T = Tangent Young’s Modulus, E_S = Secant Young’s Modulus, ν = Poisson’s ratio, σ_{peak} = peak strength, $\sigma_{confining}$ = confining pressure, β = angle of failure plane with respect to core axis, c_r = residual cohesion, ϕ_r = residual angle of friction

	GR1	GR2	GR3	GR4	GR5
E_T [GPa]	17.15	14.49	1.53	2.38	0.80
E_S [GPa]	12.07	8.07	1.00	1.83	1.16
ν	0.33	–	0.15	0.15	0.5
$\sigma_{peak}/\sigma_{confining}$ [MPa]	109.4/5	82.1/5	50.5/5	30.4/4	12.0/4 ¹
β	30	30	40	–	–
c_r [MPa]	1.21	2.05	–	2.61	4.22
ϕ_r	27.0	21.5	–	36.8	28.7

	GN1	GN2	GN3a	GN3b	GN4	GN5a	GN5b	GN5c
E_T [GPa]	6.47	0.05	0.50	1.32	0.63	0.24	0.27	0.53
E_S [GPa]	4.63	0.02	0.46	1.42	0.65	0.27	0.30	0.66
ν	0.24	0.43	0.23	0.34	–	0.35	0.38	0.25
$\sigma_{peak}/\sigma_{confining}$ [MPa]	53.9/5	10.8/5 ¹	–	7.5/1	29.3/5	16.6/5 ¹	31.5/10 ¹	54.1/20 ¹
β	60	–	–	40	–	–	–	–
c_r [MPa]	–	1.38	–	0.69	1.70	–	–	–
ϕ_r	–	10.5	–	30.0	36.1	–	–	–

¹ Stress at yield point.

4. Experimental Results for Granite-Hosted Shear Zone Samples

Axial stress-strain curves for the granite-hosted shear zone samples are presented in Fig. 9a. Results from the analysis are summarized in Table 2. The axial stress-strain curves clearly show that elastic stiffness decreases with increasing degree of tectonic overprint (i.e. increasing mica content, foliation and fragmentation intensity or “tectonic damage”), as the sampling interval moves from the strongly foliated zone (GR1) to the cohesionless zone (GR5). Non-linearity in these curves can be attributed to the closure of pre-existing fractures during the initial stages of loading and plastic yielding prior to attaining peak stress, the degree of which increases with increasing tectonic damage. As such, values calculated for Young’s modulus are seen to decrease across each shear zone subzone (Fig. 10). Schneider (1992) reports the value of Young’s modulus for intact Aar granite to be 45 GPa. This compares with a value of 17 GPa obtained in this study for the strongly foliated subzone immediately neighbouring it.

In contrast, the trend observed for the Poisson’s ratio was not as consistent (Fig. 10). The value obtained for the cohesionless zone was greatest, approaching a value of approximately 0.5, the upper limit for Poisson’s ratio indicating that the material did not change its volume. A relatively high Poisson’s ratio would also be indicative of a significant degree of plastic deformation contributing to the overall strain, bringing into question the applicability of the elastic constants (i.e. E and ν) in describing the stiffness/deformability of the highly fractured/cohesionless zone material.

In terms of peak strength, values were seen to considerably decrease with increasing tectonic overprint/damage (Figs. 9a, 10; Table 2). A 38% reduction in peak strength was seen in the strongly foliated zone, compared to the value given by

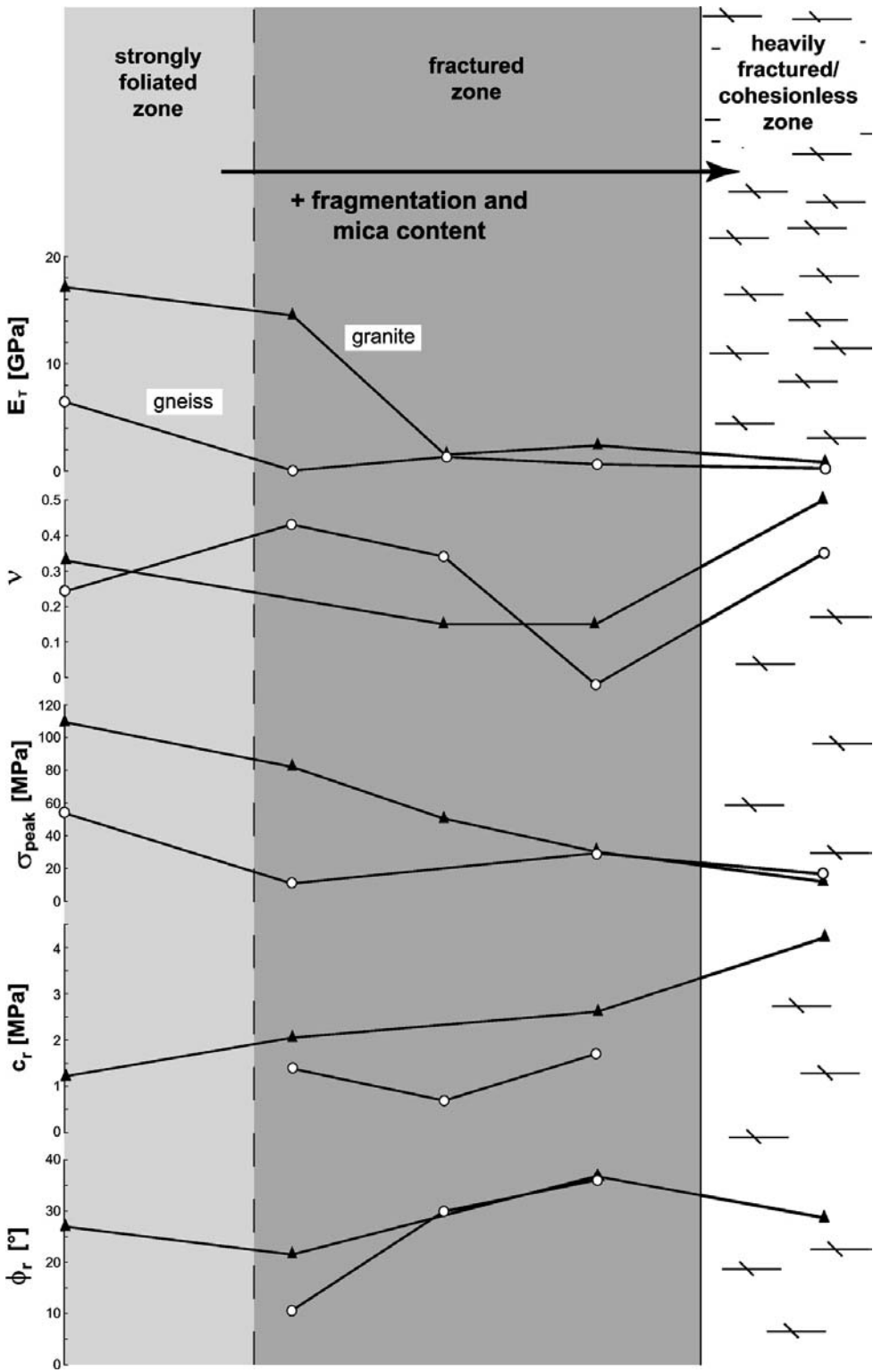


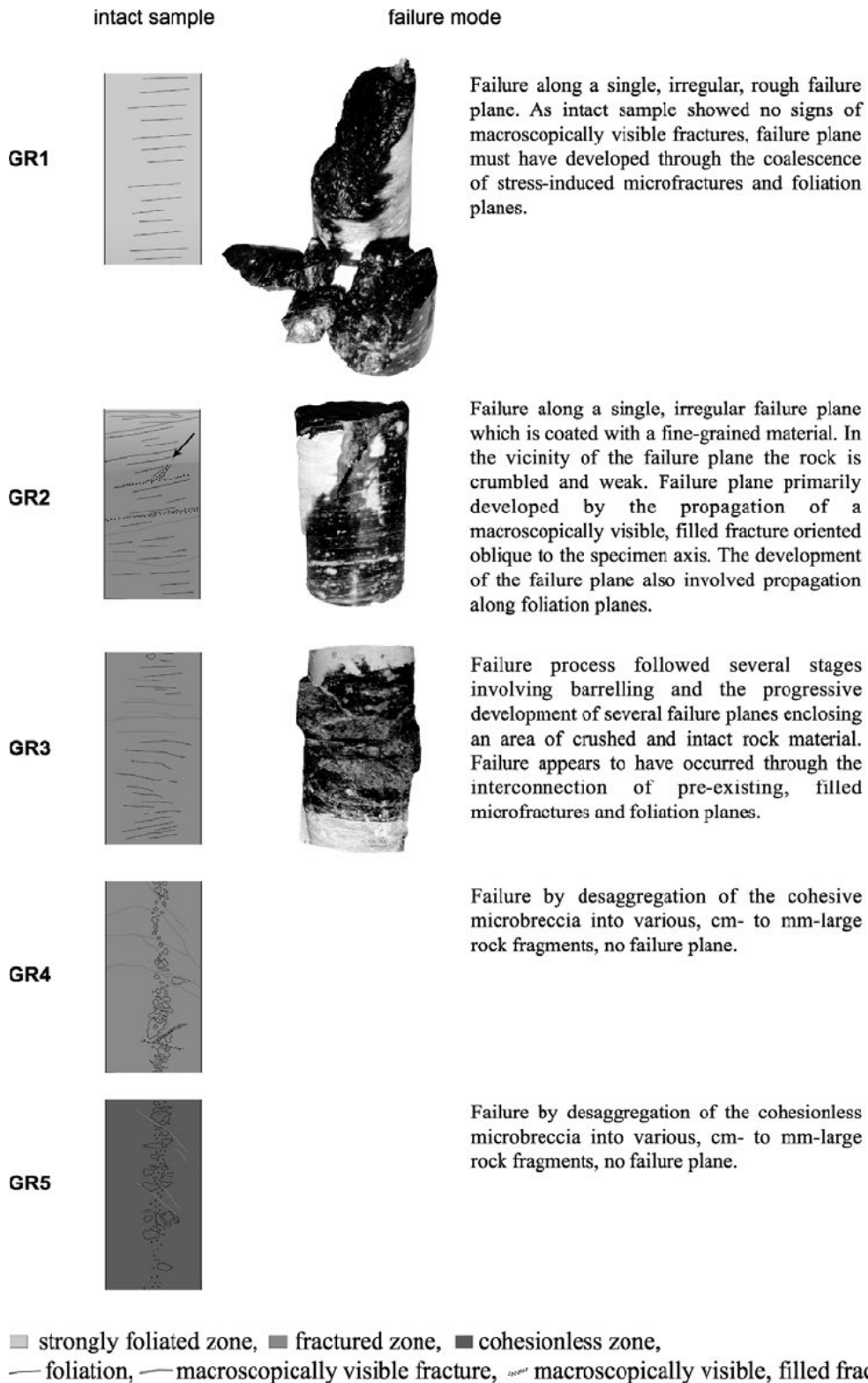
Fig. 10. Variation in tangent Young's modulus (E_T), Poisson's ratio (ν), peak strength (σ_{peak}), residual cohesion (c_r) and residual angle of internal friction (ϕ_r) with respect to the structural composition of the granite- and gneiss-hosted shear zones

Schneider (1992) for the intact, homogeneous granite host rock of 176 MPa. Additionally, the sharpness and degree of the post-peak drop in load bearing capacity from peak strength to residual strength decreased with increasing tectonic damage (Fig. 9a). For example, sample GR1, representing the least overprinted/damaged material, experienced a sharp 86% drop in strength from peak to its residual value. Post-peak drops of 82%, 74%, and 13% were observed for samples GR2, GR3 and GR4, respectively, and sample GR5, representing the heavily fractured/cohesionless zone, underwent strain hardening. The decreasing sharpness in the drops from peak to residual strength clearly implies a transition from brittle behaviour (samples GR1 and GR2) to fully ductile rock behaviour (sample GR5) with increasing tectonic overprint/damage.

This transition from brittle to ductile rock behaviour manifested through the increasing degree of plastic deformation contributing to the overall strain can likewise be related to the modes of failure observed in each of the different samples (Fig. 11). Samples GR1 and GR2 failed in a typically brittle manner with the development of a single, discrete failure plane with a 30° angle towards σ_1 (Fig. 11; Table 2). Closer observation of sample GR1 reveals that the failure plane developed through the coalescence of stress-induced microfractures, some of which developed preferentially along foliation planes. Sample GR2 failed through the propagation of a pre-existing, filled, macroscopic fracture oriented oblique to the specimen axis. Thin sections of the failed sample show that the development of the failure plane also involved the propagation of microfractures along foliation planes.

With increasing tectonic overprint/damage, though, the formation of a distinct, brittle failure plane became less prominent. In the case of sample GR3, for which the stress-strain curve showed a clear transition from brittle to ductile rock behaviour, failure occurred through barrelling and shearing along several planes. This “shearing zone” enclosed an area of crushed and intact rock material (Fig. 11), bounded by shear planes oriented at 40° to σ_1 . Thin sections analysis showed that these multiple shear planes developed through the coalescence of pre-existing microfractures and foliation planes facilitated by the high pre-testing fracture density (Fig. 13). Samples GR4 and GR5, representing those samples with the highest pre-test fracture density, failed by fragmenting into cm- to mm-sized pieces. As such, failure was predominantly ductile occurring in the form of large deformations and barrelling of the entire sample volume, accommodated by the presence of either numerous pre-existing microfractures (GR4) or almost cohesionless infill along macroscopically filled fractures (GR5).

The shift in rock behaviour from predominantly brittle to predominantly ductile failure had a significant effect on the calculated Mohr-Coulomb residual strength parameters. Residual cohesion values systematically increased with increasing tectonic overprint/damage (Figs. 16a, 10; Table 2). Similarly, values for the residual angle of internal friction also increased but not as consistently. These increases in residual strength with degree of tectonic damage signify an increased residual shear resistance along the failure plane as the formation of the failure plane varies from that of a smooth discrete plane to that of a ductile/yielding shear zone. Observations therefore suggest that an increase in load carrying capacity during post-peak deformation exists relative to that of the intact host rock with increasing degree of tectonic



■ strongly foliated zone, ■ fractured zone, ■ cohesionless zone,
 — foliation, — macroscopically visible fracture, — macroscopically visible, filled fracture

Fig. 11. Transformation from brittle to ductile failure modes for granite-hosted shear zone samples (sample diameter = 90 mm, height = 180 mm)

overprint (although the intact host rock would obviously be able to sustain higher loads before failing). Accordingly, the controlling processes and energy release rate mechanism involved in the formation of a discrete brittle failure surface (i.e. through fracture propagation and coalescence) act to eliminate/destroy almost all inherent cohesive elements existing along the path of the developing shear plane. As such, post-peak strength would only be provided in the form of frictional resistance along the discrete shear surface. In contrast, the development of a thicker “failure zone” involving a number of shear planes encompassing crushed and intact rock material would act to maintain some cohesion during post-peak deformation. Observations further demonstrate that the magnitude of the residual cohesion increases with the thickness of the yielding shear zone that develops during peak failure, as does the frictional resistance provided by the sharper, more complex asperities mixing with smaller intact rock fragments.

5. Experimental Results for Gneiss-Hosted Shear Zone Samples

Results from the tests performed on the gneiss-hosted shear zone samples show a less regular pattern than those taken from the granite-hosted shear zone (Figs. 9b, 10; Table 2). Such divergences are indicative of the more complex and heterogeneous nature of the gneiss-hosted shear zone (Fig. 5). Still, similar trends were observed in terms of the failure mode progressively changing from brittle to ductile with increasing tectonic overprint/damage. Again in a similar fashion, this shift led to a decrease in the Young’s modulus, peak strength and sharpness and magnitude of the post-peak strength drop.

Peak strength and Young’s modulus values were seen to decrease by 70% and 80%, respectively, at the transition from intact rock to the strongly foliated zone when compared to values determined by Schneider (1992) for intact biotite gneiss representative of the undamaged host rock (UCS = 167 MPa, E = 38 GPa). Poisson’s ratio values were seen to widely vary and again approached values that brought into question the applicability of elastic constants in rock materials exhibiting a high degree of plastic strain. Drops from peak to residual strength with increasing tectonic damage were measured as 16%, 4%, 25% and 11% for samples GN1, GN2, GN3b and GN4, respectively. Samples GN5a-c showed strain hardening.

Descriptions of the transition from brittle to ductile rock behaviour, as seen in the failure modes for the gneiss-hosted shear zone samples, are documented in Fig. 12. Unlike its granitic counterpart, sample GN1 representing the most competent of the gneiss-hosted shear zone rocks, did not fail along a single, discrete shear plane. Instead, failure occurred along a zone of several fractures oriented at an angle of 60° to σ_1 (Fig. 12; Table 2). Thin-section observations revealed that the formation of the failure planes involved the coalescence of pre-existing microfractures with those originating along foliation. Samples GN3b and GN4 also failed along similar failure zones, which in turn increased in thickness with increasing degree of tectonic overprint. In the case of GN3b, failure occurred through the coalescence of pre-existing, macroscopically visible fractures oriented obliquely to the sample axis. The failure zone formed in sample GN4 involved the propagation and coalescence

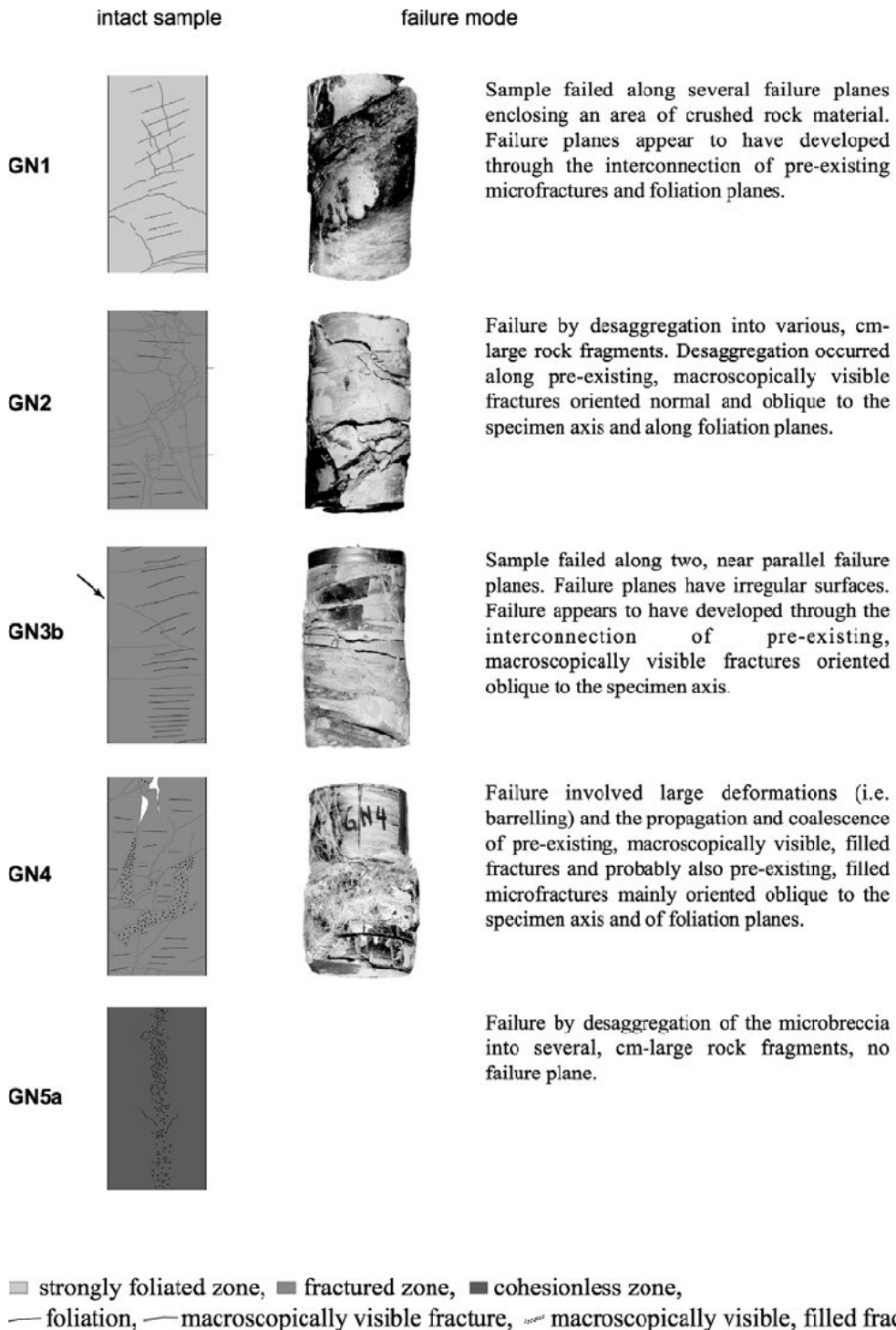


Fig. 12. Transformation from brittle to ductile failure modes for gneiss-hosted shear zone samples (approximate sample diameter = 90 mm, height = 180 mm)

of fractures initiated along pre-existing, filled macrofractures oriented obliquely to the specimen axis and foliation planes (Figs. 14, 15). Failure of sample GN4 also involved a high degree of plastic deformation leading to barrelling of the test sample (Fig. 12).

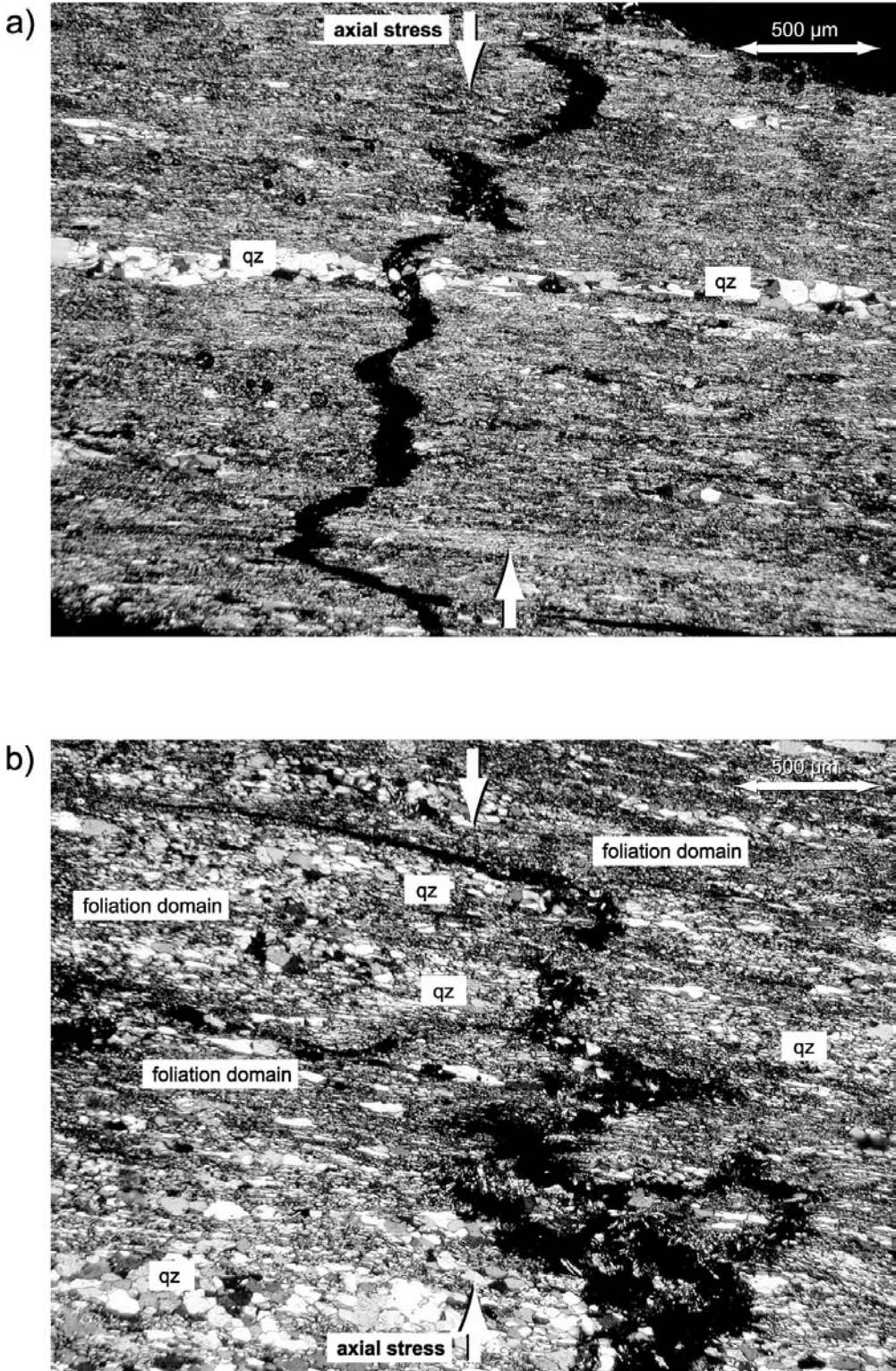


Fig. 14a,b. Thin sections taken from GN4 after testing – specifically from *barreled region* of failed sample. Photos show a transgranular fracture intersecting quartz-rich areas (*qz*) and finer-grained foliation domains. Fractures generally propagate in a direction sub-parallel to axial loading (oblique to foliation) but with interconnecting steps aligned sub-parallel to foliation. Thin sections show a cut perpendicular to foliation and parallel to stretching lineation (crossed polars)

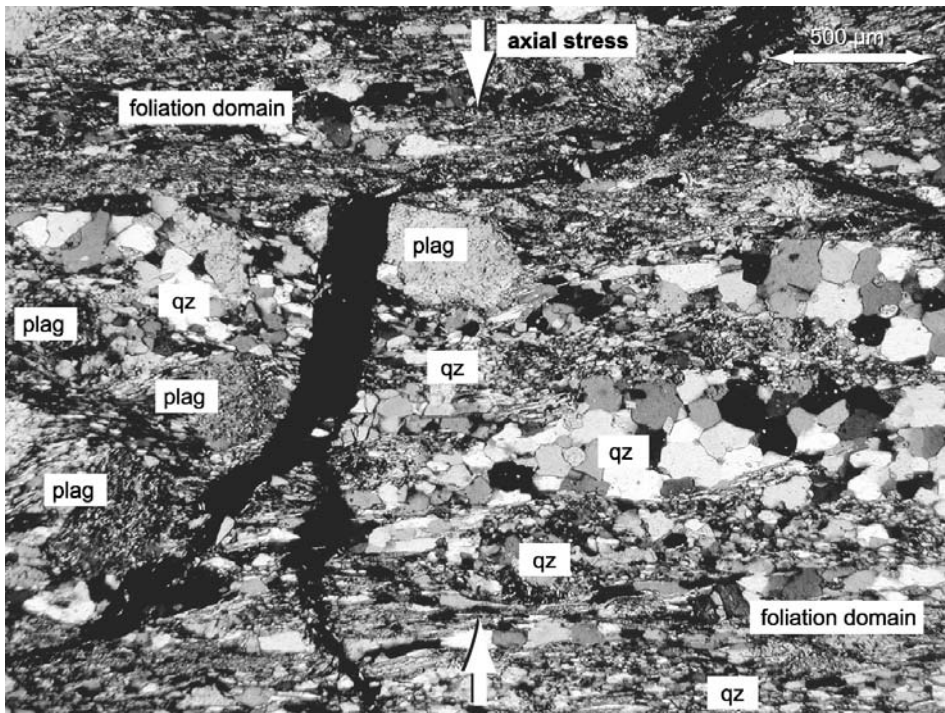


Fig. 15. Contrasting thin section taken from GN4 after testing – specifically from *non-barreled* region of failed sample. The photo shows a transgranular fracture intersecting feldspar minerals (*plag*), quartz-rich areas (*qz*) and finer-grained foliation domains. Fractures propagate in a direction sub-parallel to axial loading (oblique to foliation) with only minor stepping sub-parallel to foliation. Thin section shows a cut perpendicular to foliation and parallel to stretching lineation (crossed polars)

Figure 14 depicts the state of the material taken from the high-strain (barreled) interval and shows that this region contained a high amount of fine-grained mica and a high number of microfractures. The fractures are generally short and have extremely rough surfaces. Samples GN2 (uncharacteristically with respect to the granite-hosted results) and GN5a (characteristically) failed by preferentially fragmenting into cm-size pieces along pre-existing fractures. The failure modes again correlate well with the values of residual cohesion and residual angle of internal friction (Figs. 16b, 10; Table 2). However, the trends obtained were based on a more limited data set and are not as conclusive given the heterogeneous nature of the more highly strained and altered gneissic rock mass. In general, the gneiss-hosted shear zone material was weaker and showed less brittle rock behaviour than the granite-based samples.

6. Comparison of Experimental Results for Fault Zone Materials

Results of drained triaxial tests performed on faulted rock materials have been similarly presented (e.g. Chester and Logan, 1986; Habimana et al., 2002; Ehrbar and Pfenniger, 1999). These laboratory studies primarily differ from one another in their host rock lithology and the degree of brittle and/or ductile control. Chester and Logan (1986) tested sandstone samples from the brittle Punchbowl fault zone in California

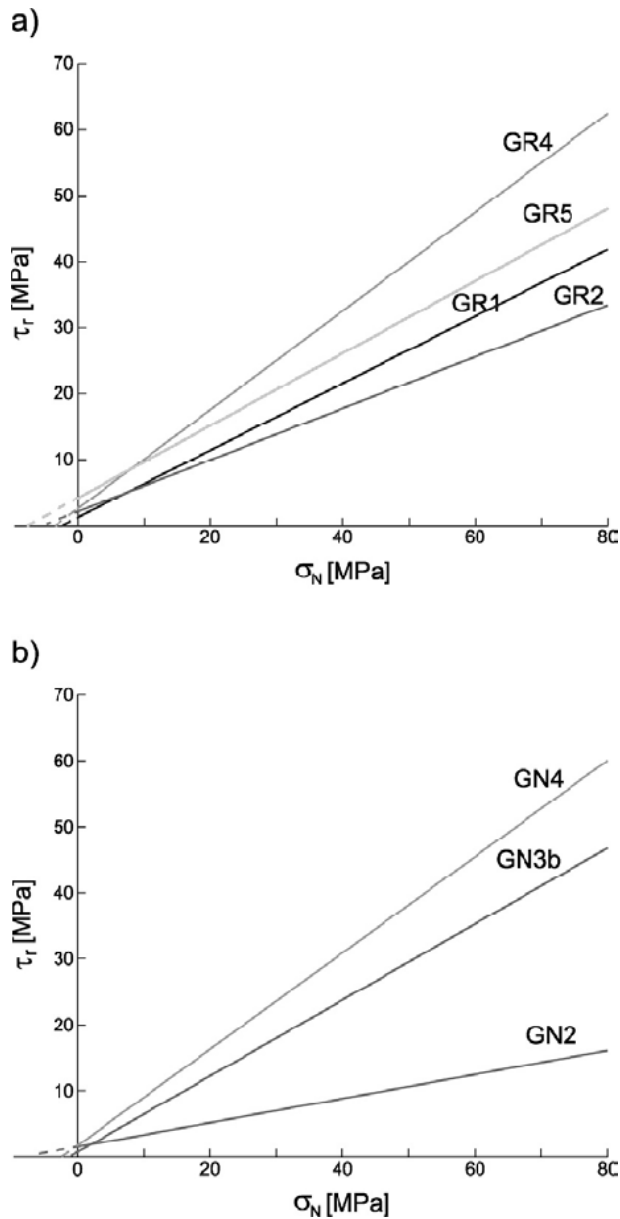


Fig. 16. Coulomb residual strength envelopes for: **a)** granite-hosted shear zone samples; **b)** gneiss-hosted shear zone samples

and defined samples as being either undisturbed, containing single and/or multiple subsidiary faults or consisting of fault gouge material. Habimana et al. (2002) tested rock material from fault zones developed in quartzitic sandstone and phyllitic schists. The samples were differentiated by the degree of folding, faulting and jointing phenomena (i.e. “tectonisation”). Faulted gneisses, schists and phyllites from the Tavetsch massif (Fig. 1) were reported by the Ehrbar and Pfenniger, 1999. The tested material was divided into slightly faulted rocks (“kakiritised” rocks), intensely faulted, fine-grained rocks with low cohesion (“regional Kakirites”) and extremely

Table 3. Comparison of elastic moduli for fault zone and fractured shear zone materials

	E-moduli [GPa]				
	Chester & Logan (1986)	Habimana et al. (1998)/ Habimana (1999)	Ehrbar & Pfenniger (1999) (phyllites)	This study (granite-hosted shear zone)	This study (gneiss-hosted shear zone)
intact material	22.5 ⁴	–	10.0 ⁵	17.1 ²	6.5 ²
increasing tectonisation ↓	22.0 ⁴	8.7 ²	8.0 ⁵	14.5 ²	–
	17.0 ⁴	5.6 ²	–	1.5 ²	1.3 ¹
	–	0.8 ³	7.5 ⁵	2.4 ²	0.6 ²
	intensely fractured material	8.5 ⁴	0.2 ²	2.0 ⁵	0.8 ²

¹ σ_{radial} = ca. 1 MPa; ² σ_{radial} = ca. 5 MPa; ³ σ_{radial} = ca. 13 MPa; ⁴ σ_{radial} = ca. 50 MPa, values for E-modulus are estimated from axial stress-strain curves; ⁵ σ_{radial} not given.

heavily faulted, very fine-grained, clay-rich, structureless and cohesionless rocks (“zonal Kakirites”).

Similarities do, however, allow for generalized comparisons to be made with respect to fracture density and its influence on test results between these different studies. As such, a comparison of Young’s moduli established in these testing campaigns and scaled with respect to fracture density is presented in Table 3. The values provided demonstrate that elastic stiffness decreases with increasing fracture density. Chester and Logan (1986) additionally describe a gradual decrease in strength and an increase in ductile rock behaviour with increasing fracture density and clay content. Similarly, Habimana et al. (2002) report a decrease in rock strength and an increase in plastic yielding with increasing degree of tectonisation, and Ehrbar and Pfenniger (1999) show a reduction in the post-peak drop from peak to residual strength with increasing fracture density.

As such, the results from these studies concur with those established herein for the eastern Aar massif shear zone rocks. Yet it should also be noted that the eastern Aar massif shear zone rocks differ from those mentioned above given their pre-brittle ductile shear zone history (i.e. their mylonitic fabric). Within this study alone, comparative differences between granite- and gneiss-hosted shear zone samples clearly demonstrate the important role foliation plays in forming preferential planes of weakness, which when later exposed to episodes of brittle deformation influenced shear zone development and accordingly, the corresponding failure mechanisms observed during testing.

7. Discussion

7.1 Strength and Deformation Characteristics of Shear Zone Samples

The triaxial tests performed demonstrated that an increasing degree of tectonic overprint/damage corresponds to: an increase in stress-strain non-linearity, a decrease in

elastic stiffness, a decrease in peak strength and an increase in residual strength. Failure modes show a transition from brittle failure along a single, discrete shear plane to ductile failure encompassing a definable yield zone, the thickness of which increases with increasing tectonic damage. These trends can be correlated to increasing densities of pre-existing planes of weakness (especially those inclined at 25–40° to σ_1), increasing thickness of fracture infill and the increase in visible mica content (Figs. 4–5, 11–12; Table 1), the propensity of which increases as a function of brittle tectonic overprinting across the *in situ* shear zone. Pre-existing planes of weakness were associable with micro- and macrofractures and foliation planes. However, as foliation planes were oriented normal to the loading direction their influence was somewhat reduced.

As such, the controlling influence of pre-existing micro- and macrofractures can be followed throughout the entire stress-strain curve. During the initial stages of loading, samples with increasing tectonic damage/fracture density would require higher stress thresholds to attain crack closure (see Eberhardt et al., 1999). This increase in the ratio of plastic to elastic strain is especially visible in the axial stress-strain curves for samples GR1 to GR3 (Fig. 9), where continuously increasing pre-test fracture densities correspond to increased non-linearity during the initial stages of loading. Subsequent to crack closure, the pre-existing fractures and foliation planes may be viewed as planes of weakness and stress concentrators along which new, stress-induced fractures may initiate, propagate and coalesce more easily, especially if they are inclined at angles greater than 25–40° with respect to the loading direction. An increasing number of pre-existing fractures, when critically stressed, would therefore lead to an increasing number of actively propagating fractures widely distributed throughout the sample. As a result, the development of plastic deformation mechanisms (e.g. slip, cataclastic flow, etc.) would be more frequently facilitated. Accordingly, increases in the amount of plastic strain during loading would correspond to decreases in the elastic stiffness, and subsequently peak strength. Thus, given the increase in fracture density, fracture infill and mica content with increasing brittle tectonic overprint/damage, moving from the host rock to the strongly foliated zone through to the heavily fractured/cohesionless zone, a full transition can be traced from typically brittle to fully ductile rock behaviour. The associated increase in the amount of plastic strain contributing to the overall deformation manifests itself in form of increased sample barrelling, as opposed to the formation of a discrete shear plane when brittle mechanisms (i.e. microfracture propagation and coalescence) dominate the failure mode.

These factors can also be used to explain the lower strengths and elastic moduli seen in the gneiss-hosted shear zone samples relative to their granitic counterparts. Higher fracture densities, foliation intensities and mica contents were seen in the gneiss-based shear zone samples (Table 1). These increases in structural complexity and heterogeneity led to several exceptions to the general trends established, most notably in sample GN2 where the presence of a higher density of long, macroscopically visible fractures (Fig. 12), led to the most ductile and weak rock behaviour encountered.

7.2 Strength and Deformability Characteristics of the Sheared Rock Mass

Laboratory observations suggest that it may be possible to assign each shear zone subzone a typical rock mass constitutive behaviour and a corresponding dominant

mode of expected failure. For example, the host rock and the strongly foliated zone would be expected to behave in a predominantly brittle manner, with failure likely involving the development of discrete shear planes with reduced residual strength bearing capacities. Tunnel convergence would not be expected to be a major factor and instability problems may be limited to wedge failures, brittle breakouts/overbreaks and/or, under high stress conditions, bursting. The neighbouring fractured zone represents a transition from brittle to ductile behaviour and failures may incorporate more yielding along a zone of finite width than along a single, discrete plane. As a result, the peak strength of these rocks would be generally lower than those of the strongly foliated zone but may carry a higher post-peak load given its greater residual strength. Material encountered in the heavily fractured, cohesionless zone would behave in a fully ductile manner. Large deformations, squeezing ground and/or the development of progressively upward unravelling chimneys may be expected. Unlike the other shear zone materials, where a strain-softening constitutive model may be adopted, this material would require a strain-hardening model.

The scale effects associated with using laboratory test values, especially where structure plays a significant controlling role, is evident. The importance and consequence of scale effects, however, is expected to diminish in the shear zone rocks as the rock quality progresses towards the heavily fractured/cohesionless zone. For example, at the laboratory scale the strongly foliated zone has a relatively low fracture density, but on the rock mass scale, it contains widely spaced, discrete, persistent joints that will locally control the rock mass behaviour. As such, the test results applied to this zone would require more attention to scale effects. Towards the cohesionless zone, as fracture density increases, the influence of individual, persistent, discrete fractures locally controlling rock mass behaviour diminishes. As such, the heavily fractured nature of the fractured zone and cohesionless zone means that their behaviour can be more easily approximated as an isotropic continuum, and therefore more closely represent the material behaviour at a larger *in situ* scale. This would seem to be true for samples GR4, GN4, GR5 and GN5a-c. In its extreme, the dimensions of samples GR5 and GN5a-c are of the same scale as the complete thickness of the cohesionless zone and may therefore be regarded as being highly representative of the rock mass scale properties for the heavily fractured/cohesionless subzone.

7.3 Hoek-Brown Strength Estimates Applied to the Sheared Rock Mass

To further derive more information with respect to the *in situ* scale rock mass properties and their variance across the shear zones, Hoek-Brown strength parameters were derived (see Hoek and Brown, 1997; Hoek et al., 1998; Hoek, 1999). The Hoek-Brown method appeared to be highly suitable given its emphasis on the role pre-existing discontinuities, joint surface roughness and fracture infill play in controlling rock mass strength.

Input values and results are given in Table 4. The general form of the Hoek-Brown criterion was used where:

$$\sigma'_1 = \sigma'_3 + \sigma_{ci} \left(m_b \frac{\sigma'_3}{\sigma_{ci}} + s \right)^a \quad (2)$$

Table 4. Input parameters and peak strengths estimated by the hoek-brown failure criterion for: a) the granite-hosted shear zone; b) the gneiss-hosted shear zone

	Strongly foliated zone			Fractured zone			Cohesionless zone		
a) granite									
σ_{ci} [MPa]	122			122			122		122
m_i	33			33			33		33
GSI	blocky/good			blocky-very blocky/good			blocky-disturbed/good		disintegrated/poor
	70			60			45		25
m_b	2.80			1.23			0.36		0.07
s	0.000464			0.000036			0.000001		0
a	0.50			0.50			0.50		0.53
σ_{peak}^1	46.41			32.40			19.82		10.64
(σ_{peak} , Laboratory)	109.4 ¹			82.1 ¹			30.4 ²		12.0 ²
b) gneiss									
σ_{ci} [MPa]	60			60			60		60
m_i	33			33			33		33
GSI	blocky-very blocky/good			blocky-disturbed/good			blocky-disturbed/good		disintegrated/good
	60			45			45		40
m_b	1.23			0.36			0.36		0.24
s	0.000036			0.000001			0.000001		0.00000002
a	0.50			0.50			0.50		0.50
σ_{peak}^1	24.21			15.39			20.69		13.49
(σ_{peak} , Laboratory)	53.9 ¹			10.8 ¹			29.3 ¹		16.6 ¹

¹ $\sigma_{radial} = 5$ MPa; ² $\sigma_{radial} = 4$ MPa; ³ $\sigma_{radial} = 1$ MPa.

and, assuming Geological Strength Indexes (GSI) greater than 25:

$$\frac{m_b}{m_i} = \exp\left(\frac{GSI - 100}{28}\right) \quad (3)$$

$$s = \exp\left(\frac{GSI - 100}{9}\right) \quad (4)$$

where σ'_1 and σ'_3 are the effective major and minimum principal stresses, m_b and m_i are constants for the rock mass and intact rock, respectively, s and a are constants dependent on the characteristics of the rock mass and σ_{ci} is the uniaxial compressive strength of the intact rock. For the calculations performed, σ_{ci} was based on peak strength values obtained for the strongly foliated zone (GR1 and GN1). The value of m_i was estimated as that for foliated gneiss, as given in the table provided by Hoek et al. (1995). The different shear zone subzones were characterized using the Geological Strength Index (GSI), as described in Hoek et al. (1998) and Hoek (1999). As shown in Table 4, several different rock strength values were estimated for the fractured zone given the strong increase in fracture density across this zone. Estimates of the fracture surfaces were taken as “good” as described in Hoek et al. (1995), given that most surfaces were relatively rough (Fig. 2b) and infills were relatively thin and compact.

The resulting estimates of rock mass strength (σ_{peak} in Table 4) reflect the variations in peak strength values observed in the laboratory, showing decreases with increasing fracture density. However, the estimated rock mass strength of the granitic-based strongly foliated zone was found to be less than half the laboratory value. This discrepancy between Hoek-Brown rock mass values and laboratory determined values decreases with increasing tectonic damage and converges towards the cohesionless zone, where strengths are approximately the same. Rock strengths for the gneiss-hosted shear zone materials show a similar trend. It should be noted that the 50% difference between laboratory and rock mass compressive strength values for the strongly foliated zone corresponds to the general rule of thumb used in mining and tunnelling. The convergence of these values with increasing tectonic damage, confirms the assumption that as test samples approach the cohesionless zone, they become more and more representative of the rock mass behaviour (i.e. as fracture density increases and the influence of discrete, persistent discontinuities decreases).

8. Conclusions

Results from this study show:

1. Rock mass strength and deformability within shear zones in the eastern Aar massif are related to their complex, multiphase structural characteristics. The geomechanical properties are mainly influenced by fracture density, foliation intensity, thickness of fine-grained fracture infill and mica content.
2. With increasing fracture density and mica content, the shear zones in the eastern Aar massif can be divided into a strongly foliated zone, a fractured zone and a heavily fractured/cohesionless zone. In this respect, it is possible to assign each

subzone a characteristic rock mass constitutive behaviour and a controlling mode of failure:

- The *strongly foliated zone* neighbouring the host rock can be expected to behave in a predominantly brittle manner and fail along a single, discrete shear plane with a higher peak strength but relatively low residual strength.
 - The *fractured zone* represents a transition from brittle to ductile behaviour and can be expected to fail through the development of a yielding shear zone of lower peak strength but with a higher residual strength.
 - Material from the *heavily fractured, cohesionless zone* can be expected to behave in a fully ductile manner and fail through large deformations in the form of barrelling over the whole sample volume, while simultaneously undergoing strain hardening.
3. As fracture density increases and the influence of discrete, persistent discontinuities on rock mass strength decreases, behaviour of the test samples becomes more and more representative of the *in situ* rock mass behaviour. Heavily fractured and fragmented test samples may be regarded as an isotropic continuum and representative of the rock mass itself.

The gradual degradation in rock stiffness and strength observed in the different test samples can have significant practical implications with respect to ongoing and future tunnelling projects in the Swiss Alps and elsewhere. The high density of fractures parallel and oblique to the foliation, particularly within the fractured and almost cohesionless intervals of the shear zone, implies that in lower stress environments increased ground control problems may be encountered in the form of unravelling interlocked blocks and wedges (i.e. structurally controlled instability). The size of the blocks and wedges should generally decrease as foliation and fracture intensity increases. This process would likely be progressive in nature, starting with the unravelling of smaller blocks exposed at the excavation surface and gradually working its way back into the rock mass. Such trends would correlate with observations made during the construction of the Gotthard highway tunnel where steeply dipping fractured and almost cohesionless shear zone intervals were intersected and progressive instabilities developed both at the tunnel face and in the tunnel roof.

In higher stress environments, results from this study would suggest that along the less tectonically damaged rock mass intervals, failure would predominantly occur through sliding along discontinuities and/or spalling of intact rock pieces (i.e. stress controlled instability). Along more heavily fractured sections of the shear zone, increased plastic yielding may result in floor heave and sidewall closure (i.e. squeezing). High pore water pressures would only further aggravate the situation and act to increase the magnitude of the resulting displacements.

As such, the selection of tunnelling/excavation method, the use of numerical models and the design of adequate support measures in such geological environments, must consider and include the variability of the sheared rock mass behaviour with respect to the degree of tectonic overprint/damage, and the respective problematic implications the response of these materials may have when intersected during tunnelling.

Acknowledgements

The authors would like to thank the maintenance team of the Gotthard highway tunnel in Göschenen for providing access and support for the work performed in their safety tunnel. J.-F. Mathier and J. Mottier are thanked for their technical assistance in performing the laboratory tests. This project was financed by an ETHZ research grant (ETH-Project Nr. 01122/41-2704.5).

References

- Abrecht, J. (1994): Geologic units of the Aar massif and their pre-alpine rock associations: a critical review. *Schweiz. Mineral. Petrogr. Mitt.* 74, 5–27.
- Bossart, P., Mazurek, M. (1990): Strukturgeologische Charakterisierung und Geometrie der Wasser fließwege in der Migrationsscherzone VT 420, Felslabor Grimsel. NAGRA Internal Report #90–44.
- Brady, B. H. B., Brown, E. T. (1993): *Rock mechanics for underground mining*, 2nd edn. Chapman & Hall, London.
- Chester, F. M., Logan, J. M. (1986): Implications for mechanical properties of brittle faults from observations of the Punchbowl Fault Zone, California. *Pure Appl. Geophys.* 124, 79–106.
- Choukroune, P., Gapais, D. (1983): Strain patterns in the Aar Granite (Central Alps): Orthogneiss developed by bulk inhomogeneous flattening. *J. Struct. Geol.* 5, 411–418.
- Davis, G. H., Reynolds, S. J. (1996): *Structural geology of rocks and regions*. Wiley & Sons, New York.
- Deere, D. U. (1973): Foliation shear zones – an adverse engineering geologic feature of metamorphic rocks. *J. Boston Soc. Civil Eng.* 60/4, 163–176.
- Eberhardt, E., Stead, D., Stimpson, B. (1999): Effects of sample disturbance on the stress-induced microfracturing characteristics of brittle rock. *Can. Geotech. J.* 36, 239–250.
- Eckardt, P. M. (1957): Zur Talgeschichte des Tavetsch, seine Bruchsysteme und jungquartären Verwerfungen. Ph.D. thesis, University of Zürich, Switzerland.
- Eckardt, P., Funk, H., Labhart, T. (1983): Postglaziale Krustenbewegungen an der Rhein-Rhone-Linie. *Vermessung, Photogrammetrie, Kulturtechnik* 2, 43–56.
- Ehrbar, H., Pfenniger, I. (1999): Umsetzung der Geologie in technische Maßnahmen im Tavetscher Zwischenmassiv Nord. In: Loew, S., Wyss, R. (eds.) *Vorerkundung und Prognose der Basistunnels am Gotthard und am Lötschberg*. A.A. Balkema, Rotterdam, 381–394.
- Fischer, W. (1990): Verschiebungsmessungen im Gebiet Stöckli-Lutersee, Arbeiten 1975–1990, Dokumentation der Anlage. ETH Zürich, Institut für Geodäsie und Photogrammetrie, Bericht 175.
- Frey, M., Bucher, K., Frank, E., Mullis, J. (1980): Alpine metamorphism along the geotraverse Basel-Chiasso – a review. *Eclogae Geol. Helv.* 73, 527–546.
- Gubler, E., Kahle, H. G., Klingelé, E., Mueller, S., Olivier, R. (1981): Recent crustal movements in Switzerland and their geophysical interpretation. *Tectonophysics* 71, 125–152.
- Habimana, J., Labiouse, V., Descoedres, F. (2002): Geomechanical characterisation of cataclastic rocks: experience from the Cleuson-Dixence project. *Int. J. Rock Mech Min. Sci.* 39, 677–693.
- Higgins, M. W. (1971): *Cataclastic rocks*. Professional Paper, U.S. Geological Survey #687.
- Hoek, E. (1999): Putting numbers to geology – an engineer's viewpoint. *Quart. J. Eng. Geol.* 32, 1–19.

- Hoek, E., Brown, E. T. (1997): Practical estimates of rock mass strength. *Int. J. Rock Mech. Min. Sci. Geomech. Abstr.* 34, 1165–1186.
- Hoek, E., Kaiser, P. K., Bawden, W. F. (1995): Support of underground excavations in hard rock. A.A. Balkema, Rotterdam.
- Hoek, E., Marinos, P., Benissi, M. (1998): Applicability of the geological strength index (GSI) classification for very weak and sheared rock masses: the case of the Athens schist formation. *Bull. Eng. Geol. Environ.* 57, 151–160.
- Hulin, C. D. (1929): Structural control of ore deposition. *Economic Geol.* 24, 15–49.
- ISRM (1983): International Society for Rock Mechanics suggested methods for determining the strength of rock materials in triaxial compression (revised version). *Int. J. Rock Mech. Min. Sci. Geomech. Abstr.* 20, 283–290.
- Jäckli, H. (1951): Verwerfungen jungquartären Alters im südlichen Aarmassiv bei Somvix-Rabius (Graubünden). *Eclogae Geol. Helv.* 44, 332–337.
- Kahle, H.-G., Geiger, A., Bürki, B., Gubler, E., Marti, U., Wirth, B., Rothacher, W., Gurtner, W., Beutler, G., Bauersima, I., Pfiffner, O. A. (1997): Recent crustal movements, geoid and density distribution: contribution from integrated satellite and terrestrial measurements. In: Pfiffner, O. A., Lehner, P., Heitzmann, P., Mueller, S., Steck, A. (eds.) *Results of NRP 20: Deep Structure of the Swiss Alps*. Birkhäuser Verlag, Basel, 251–259.
- Keller, F., Schneider, T. R. (1982): Der Furka-Basistunnel, Geologie und Geotechnik. Schweiz. Ingenieur Architekt 24.
- Keller, F., Wanner, H., Schneider, T. R. (1987): Geologischer Schlussbericht Gotthard-Strassentunnel, Zusammenfassung. Beiträge zur Geologie der Schweiz, Geotechnical Series 70.
- Kovári, K., Tisa, A. (1975): Multiple failure state and strain controlled triaxial tests. *Rock Mech.* 7, 17–33.
- Labhart, T. P. (1977): Aarmassiv und Gotthardmassiv, Sammlung geologischer Führer, Volume 63. Gebr. Bornträger, Berlin.
- Laws, S., Loew, S., Burg, J.-P. (2003): Structural characterization of shear zones in the Eastern Aar Massif, Switzerland. Submitted to *Eclogae Geol. Helv.*
- Loew, S., Ziegler, H.-J., Keller, F. (2000). Alptransit: engineering geology of the world's longest tunnel system. *GeoEng 2000: An International Conference on Geotechnical & Geological Engineering*, Melbourne. Technomic Publishing, Lancaster, 927–937.
- Meyer, J., Mazurek, M., Alexander, W. R. (1989): Petrographic and mineralogical characterisation of fault zones AU 96 and AU 126. In: Bradbury, M. H. (ed.) Paul Scherrer Institut, Programm Entsorgung, Laboratory Investigations in Support of the Migration Experiments at the Grimsel Test Site, 3–25.
- Müller, L. (1978): Der Felsbau, 3rd edn; Tunnelbau. Enke Verlag, Stuttgart.
- Passchier, C. W., Trouw, R. A. J. (1996): *Microtectonics*. Springer, Berlin Heidelberg New York Tokyo.
- Pavoni, N. (1979): Investigation of recent crustal movements in Switzerland. In: Müller, S., Oberholzer, W. F. (eds.) *International Geodynamics Project, Final Report of Switzerland*. Schweiz. Mineral. Petrogr. Mitt. 59, 117–126.
- Ramsay, J. G., Huber, M. (1987): *The techniques of modern structural geology*, Vol. II. Academic Press, London.
- Schneider, T. R. (1992): Bundesamt für Verkehr, AlpTransit, Achse Gotthard, Gotthard-Basistunnel, Aufarbeitung der felsmechanischen Grundlagen, Report 425pp.

- Schneider, T. R. (1993): Geologische Vorerkundung "Gotthard-Basistunnel". In: Schweizer Alpen-Basistunnels. Mitteilungen der Schweizerischen Gesellschaft für Boden- und Felsmechanik, Herbsttagung, 23. September 1993, Kandersteg, 53–63.
- Schubert, W. (1993): Erfahrungen bei der Durchörterung von Störzonen bei Österreichischen Tunneln. Felsbau 11, 287–290.
- Schubert, W., Riedmüller, G. (1997): Influence of faults on tunnelling. Felsbau 15, 483–488.
- Schubert, W., Riedmüller, G. (2000): Tunnelling in fault zones – state of the art in investigation and construction. Felsbau 18/2, 7–15.
- Shah, S., Hoek, E. (1991): ROCKDATA, v. 2.0 users manual: computer program to analyze laboratory strength data. Rock Engineering Group, Department of Civil Engineering, University of Toronto.
- Sibson, R. H. (1977): Fault rocks and fault mechanisms. J. Geol. Soc. London 133, 191–213.
- Steck, A. (1968a): Die alpidischen Strukturen in den zentralen Aaregraniten des westlichen Aarmassivs. Eclogae Geol. Helv. 61, 19–48.
- Steck, A. (1968b): Junge Bruchsysteme in den Zentralalpen. Eclogae Geol. Helv. 61, 387–393.
- Steck, A. (1984): Structures de déformations tertiaires dans les Alpes Centrales (transversale Aar-Simplon-Ossola). Eclogae Geol. Helv. 77, 55–100.
- Wise, D. U., Dunn, D. E., Engelder, J. T., Geiser, P. A., Hatcher, R. D., Kish, S. A., Odom, A. L., Schamel, S. (1984): Fault-related rocks: suggestions for terminology. Geology 12, 391–394.

Author's address: Dr. S. Laws, Dr. Heinrich Jäckli AG, Albulastrasse 55, CH-8048 Zürich, Switzerland. E-mail: laws@jaeckli.ch